An Immersed-Boundary Finite-Volume Method for Simulation of Heat Transfer in Complex Geometries

Jungwoo Kim, Haecheon Choi*
School of Mechanical and Aerospace Engineering, Seoul National University, Seoul 151-744, Korea

An immersed boundary method for solving the Navier-Stokes and thermal energy equations is developed to compute the heat transfer over or inside the complex geometries in the Cartesian or cylindrical coordinates by introducing the momentum forcing, mass source/sink, and heat source/sink. The present method is based on the finite volume approach on a staggered mesh together with a fractional step method. The method of applying the momentum forcing and mass source/sink to satisfy the no-slip condition on the body surface is explained in detail in Kim, Kim and Choi (2001, Journal of Computational Physics). In this paper, the heat source/sink is introduced on the body surface or inside the body to satisfy the iso-thermal or iso-heat-flux condition on the immersed boundary. The present method is applied to three different problems : forced convection around a circular cylinder, mixed convection around a pair of circular cylinders, and forced convection around a main cylinder with a secondary small cylinder. The results show good agreements with those obtained by previous experiments and numerical simulations, verifying the accuracy of the present method.

Key Words : Immersed Boundary Method, Heat Transfer, Finite Volume Method, Complex Geometry

1. Introduction

The ability to handle complex geometries has been one of the main issues in computational fluid dynamics because most engineering problems encounter difficulties in handling them. So far, two different approaches of simulating complex flow have been taken : unstructured grid method and immersed boundary method. In the latter method (Peskin, 1982 ; Goldstein et al., 1993 ; Saiki and Biringen, 1996 ; Mohd-Yusof, 1997; Fadlun et al., 2000 ; Kim et al. 2001 ; Lee, 2003), a body in the flow field is considered as a kind of momentum forcing in the Navier-Stokes equations rather than a real body, and therefore flow over a complex geometry can be easily handled with orthogonal (Cartesian or cylindrical) grids which generally do not coincide with the body surface. The main advantages of the immersed boundary method are memory and CPU savings and easy grid generation compared to the unstructured grid method. Even moving-body problems can be handled with the immersed boundary method without regenerating grids in time, unlike the unstructured grid method. Recently, Kim et al.(2001) suggested a modified immersed boundary method that introduces the momentum forcing in the Navier-Stokes equations and the mass source/sink in the continuity equation to satisfy the no-slip condition on the immersed boundary and the mass conservation for the cell containing the immersed boundary. Here the momentum forcing and mass source/sink are applied only on the body surface or inside the body.

* Corresponding Author,
E-mail : choi@socrates.snu.ac.kr
TEL : +82-2-880-8361; **FAX** : +82-2-878-3662
School of Mechanical and Aerospace Engineering, Seoul National University, Seoul 151-744, Korea.
(Manuscript **Received** November 14, 2003; **Revised** March 5, 2004)

So far, immersed boundary methods have been applied mostly to the flow field, but little attention has been paid to the passive-scalar field. Recently, using an immersed boundary method, Fadlun et al.(2000) computed the passive scalar and compared the simulation results to those from the previous experiments. As they reported, however, the adiabatic condition on the immersed boundary was hard to accurately be satisfied using their method.

In the present study, we suggest an immersed boundary method, where the thermal boundary conditions such as the iso-thermal and iso-heat-flux conditions are accurately satisfied on the immersed boundary by applying the heat source/sink on the boundary or inside the body. The present method is based on a finite volume approach on a staggered mesh together with a fractional step method. To verify the accuracy of the present method, three different heat-transfer problems are considered and the results are presented in this paper.

2. Numerical Method

2.1 Governing equations and time integration

Following Kim et al.(2001), both the momentum forcing and mass source/sink are applied on the body surface or inside the body in order to satisfy the no-slip condition on the immersed boundary and the mass conservation for the cell containing the immersed boundary. In the present study, the heat source/sink is applied to satisfy the thermal boundary conditions such as the iso-thermal and iso-heat-flux conditions on the immersed boundary. As shown in Fig. 1, the momentum forcing (f_i), mass source/sink (q) and heat source/sink (h) are applied on the immersed boundary or inside the body to properly represent the immersed body. The grid points for the momentum forcing are located in a staggered fashion like the velocity components defined on a staggered grid. Also, the grid points for the mass and heat source/sink are located at the cell centers like the pressure and temperature. Therefore, the governing equations

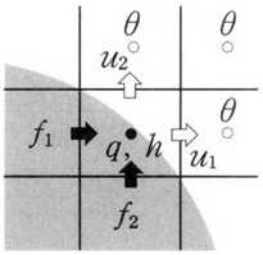

Fig. 1 Schematic diagram for the immersed boundary method. The shaded area denotes the body

for unsteady incompressible viscous flow and heat transfer become

$$\frac{\partial u_i}{\partial t}+\frac{\partial u_i u_j}{\partial x_j} = -\frac{\partial p}{\partial x_i}+\frac{1}{\mathrm{Re}}\frac{\partial^2 u_i}{\partial x_j \partial x_j}+\frac{\mathrm{Gr}\theta}{\mathrm{Re}^2}+f_i \tag{1}$$

$$\frac{\partial u_i}{\partial x_i}-q=0 \tag{2}$$

$$\frac{\partial \theta}{\partial t}+\frac{\partial u_j \theta}{\partial x_j}=\frac{1}{\mathrm{RePr}}\frac{\partial^2 \theta}{\partial x_j \partial x_j}+h \tag{3}$$

where x_i's are the Cartesian coordinates, u_i's are the corresponding velocity components, p is the pressure and θ is the temperature. All the variables are nondimensionalized by the characteristic velocity, length and temperature. Re is the Reynolds number, Pr is the Prandtl number and Gr is the Grashof number.

A second-order semi-implicit time advancement scheme (a third-order Runge-Kutta method (RK3) for the convection terms and the Crank-Nicolson method for the diffusion terms) is used for the time integration of Eqs. (1), (2) and (3). Also, we use the fractional step method where a pseudo-pressure is used to correct the velocity field so that the continuity equation is satisfied at each computational time step. Then, Eqs. (1)-(3) become

$$\begin{aligned}\frac{\hat{u}_i^k-u_i^{k-1}}{\Delta t} &= \frac{\alpha_k}{\mathrm{Re}}L(\hat{u}_i^k)+\frac{\alpha_k}{\mathrm{Re}}L(u_i^{k-1}) \\ &\quad -2\alpha_k\frac{\partial p^{k-1}}{\partial x_i}-\gamma_k N(u_i^{k-1})-\rho_k N(u_i^{k-2}) \\ &\quad +\gamma_k\frac{\mathrm{Gr}\theta^{k-1}}{\mathrm{Re}^2}+\rho_k\frac{\mathrm{Gr}\theta^{k-2}}{\mathrm{Re}^2}+f_i^k\end{aligned} \tag{4}$$

$$\frac{\partial^2 \phi^k}{\partial x_i \partial x_i} = \frac{1}{2\alpha_k \Delta t}\left(\frac{\partial \hat{u}_i^k}{\partial x_i} - q^k\right) \tag{5}$$

$$u_i^k = \hat{u}_i^k - 2\alpha_k \Delta t \frac{\partial \phi^k}{\partial x_i} \tag{6}$$

$$p^k = p^{k-1} + \phi^k - \frac{\alpha_k \Delta t}{\mathrm{Re}} \frac{\partial^2 \phi^k}{\partial x_j \partial x_j} \tag{7}$$

$$\frac{\theta^k - \theta^{k-1}}{\Delta t} = \frac{\alpha_k}{\mathrm{RePr}} L(\theta^k) + \frac{\alpha_k}{\mathrm{RePr}} L(\theta^{k-1}) - \gamma_k N(\theta^{k-1}) - \rho_k N(\theta^{k-2}) + h^k \tag{8}$$

where $L() = \partial^2()/\partial x_j \partial x_j$, $N() = \partial u_j()/\partial x_j$, $\hat{u}_i$ is the intermediate velocity, ϕ is the pseudo-pressure, Δt and k (=1, 2, 3) are the computational time step and substep's index, respectively. α_k, γ_k, ρ_k are the coefficients of RK3 ($\alpha_1 = 4/15$, $\gamma_1 = 8/15$, $\rho_1 = 0$; $\alpha_2 = 1/15$, $\gamma_2 = 5/12$, $\rho_2 = -17/60$; $\alpha_3 = 1/6$, $\gamma_3 = 3/4$, $\rho_3 = -5/12$). Here, f_i, q and h are defined inside the immersed body or on the cell containing the immersed boundary, and zero elsewhere.

The method of determining f_i and q is fully described in Kim et al.(2001). Thus, in this paper, we present the procedure of determining h of satisfying the iso-thermal and iso-heat-flux conditions on the immersed boundary.

2.2 Iso-thermal condition

To obtain θ^k from Eq. (8), the heat source/sink h^k must be determined in advance such that θ^k satisfies the iso-thermal condition on the immersed boundary. In order to obtain h^k from the velocity and temperature at $k-1$ and $k-2$ steps, we integrate Eq. (3) explicitly in time (RK3 for the convection terms and the forward Euler method for the diffusion terms) near the immersed boundary, and the resulting temperature is denoted as $\tilde{\theta}^k$:

$$\frac{\tilde{\theta}^k - \theta^{k-1}}{\Delta t} = \frac{2\alpha_k}{\mathrm{RePr}} L(\theta^{k-1}) - \gamma_k N(\theta^{k-1}) - \rho_k N(\theta^{k-2}) + h^k \tag{9}$$

Then, h^k becomes

$$h^k = \frac{\Theta^k - \theta^{k-1}}{\Delta t} - \frac{2\alpha_k}{\mathrm{RePr}} L(\theta^{k-1}) + \gamma_k N(\theta^{k-1}) + \rho_k N(\theta^{k-2}) \tag{10}$$

where $\Theta^k (= \tilde{\theta}^k)$ is the temperature at the heat source/sink location that we want to obtain by applying h^k. When the location for h^k coincides with the immersed boundary, Θ^k is the temperature given by the iso-thermal condition on the boundary. However, in general the location for h^k does not coincide with the boundary, and thus an interpolation from neighboring temperatures should be required to obtain Θ^k at the heat source/sink location. Since the neighboring temperatures should be the ones at the k-th step, they ($\tilde{\theta}$) are also obtained from Eq. (9) with $h^k = 0$.

For the interpolation scheme, we use second-order bilinear and linear interpolations as shown in Figs. 2(a) and 2(b), respectively. Here, P_1 is the location at which the iso-thermal condition should be satisfied, and Θ_1, $\tilde{\theta}_2$ (or Θ_2), $\tilde{\theta}_3$ and $\tilde{\theta}_4$ are the temperatures nearby P_1. P_1 is defined as the cross-sectional point between the immersed boundary and the wall-normal line passing through the point where Θ_1 is defined. When all the temperature points ($\tilde{\theta}_2$, $\tilde{\theta}_3$ and $\tilde{\theta}_4$) except Θ_1 are outside the body (Fig. 2(a)), Θ_1 is determined from a bilinear interpolation. However, when Θ_1 and Θ_2 are inside the immersed body as shown in Fig. 2(b), Θ_1 cannot be determined from the bilinear interpolation because the unknown Θ_1 is coupled with another unknown Θ_2. In this case, we obtain Θ_1 from the linear interpolation between the temperature at P_2 and $\tilde{\theta}_4$, where P_2 is the cross-sectional point between the immersed boundary and the line connecting Θ_1 and $\tilde{\theta}_4$.

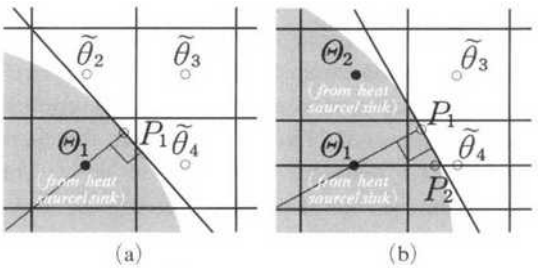

Fig. 2 Schematic diagram for the interpolation scheme in the case of iso-thermal condition: (a) Bilinear interpolation; (b) Linear interpolation. The shaded area denotes the body

We now explain the linear and bilinear interpolation schemes in more detail in Figs. 3 and 4, respectively. To simplify the problem, the case of $\theta=0$ at the boundary is considered and the case of $\theta\neq 0$ at the boundary can be easily extended from that of $\theta=0$. First, we consider the following second-order linear interpolation (Fig. 3)

$$\Theta_1^k=-\tilde{\theta}_{C'}^k \tag{11}$$

where C' is defined such that $\overline{C'P_2}=\overline{P_2C}=l$. For $0<l\leqq y_A$ (Fig. 3(a)), $\tilde{\theta}_{C'}^k$ is obtained from a linear interpolation between $\tilde{\theta}_A^k$ and the temperature condition at P_2, whereas for $y_A<l\leqq y_B$ (Fig. 3(b)), $\tilde{\theta}_{C'}^k$ is obtained from $\tilde{\theta}_A^k$ and $\tilde{\theta}_B^k$. That is,

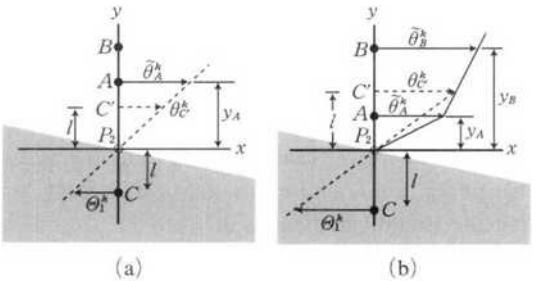

Fig. 3 Linear interpolation scheme in the case of iso-thermal condition: (a) $0<l\leqq y_A$; (b) $y_A<l\leqq y_B$. Here, C is the heat source/sink point, and C' is defined such that $\overline{C'P_2}=\overline{P_2C}=l$. A and B are, respectively, the first and second temperature points (cell centers) outside the body. The shaded area denotes the body

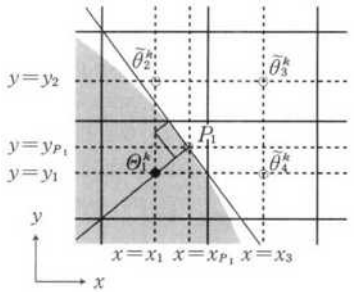

Fig. 4 Bilinear interpolation scheme in the case of iso-thermal condition. The shaded area denotes the body

$$\Theta_1^k=\begin{cases}-\dfrac{1}{y_A}\tilde{\theta}_A^k & \text{for } 0<l\leqq y_A\\[2ex] -\dfrac{(y_B-l)\,\tilde{\theta}_A^k+(l-y_A)\,\tilde{\theta}_B^k}{y_B-y_A} & \text{for } y_A<l\leqq y_B\end{cases} \tag{12}$$

This linear interpolation procedure is same as that used for the velocity components to satisfy the no-slip condition in Kim et al.(2001). When $\Theta_1^k=-(l/y_A)\,\tilde{\theta}_A^k$ is used even for $y_A<l\leqq y_B$, one may fail to get a stable solution due to a very large value of l/y_A from the grid distribution in complex geometries.

Next, in the case of Fig. 2(a), the second-order bilinear interpolation is used as follows (see Fig. 4):

$$\begin{aligned}\Theta_1^k=-[&\alpha(1-\beta)\,\tilde{\theta}_2^k+(1-\alpha)\,(1-\beta)\,\tilde{\theta}_3^k\\&+(1-\alpha)\,\beta\tilde{\theta}_4^k]/\alpha\beta\end{aligned} \tag{13}$$

where $\alpha=(x_3-x_{P_1})/(x_3-x_1)$, $\beta=(y_2-y_{P_1})/(y_2-y_1)$, and the iso-thermal boundary condition at P_1 is used.

Once Θ_1^k is determined, h^k of satisfying the iso-thermal condition is obtained from Eq. (10).

2.3 Iso-heat-flux condition

In the case of iso-heat-flux condition, the interpolation procedure for determining Θ (or Θ^k) is different from that for the iso-thermal condition, because the iso-heat-flux condition requires the wall-normal derivative of temperature on the immersed boundary.

Figure 5 shows the schematic diagram for the interpolation scheme used in the present study. Here, P_1 is the point at which the iso-heat-flux condition should be satisfied, and Θ_1, $\tilde{\theta}_2$ (or Θ_2), $\tilde{\theta}_3$ and $\tilde{\theta}_4$ (or Θ_4) are the temperatures nearby P_1. P_1 is defined as the cross-sectional point between the immersed boundary and the wall-normal line passing through the point where Θ_1 is defined. Also, $\tilde{\theta}_5$ is the temperature at the cross-sectional point between the line connecting the cell centers and the wall-normal line as shown in Fig. 5. Then, the heat flux q'' on the immersed boundary is defined as $q''=-\kappa(\tilde{\theta}_5-\Theta_1)/\Delta n$, where κ is the conduction coefficient, Δn is the distance between the points defined for Θ_1 and $\tilde{\theta}_5$. Therefore, Θ_1^k is given as

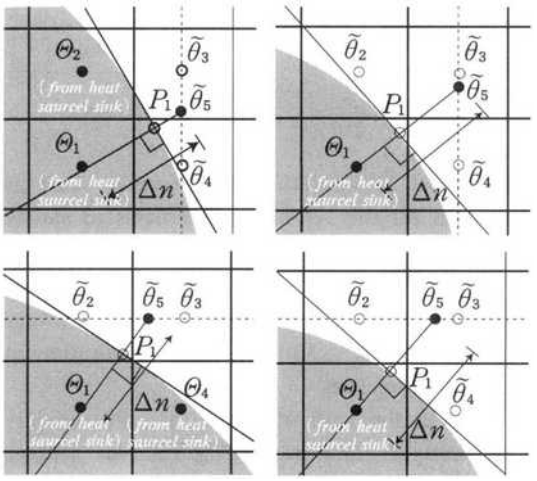

Fig. 5 Schematic diagram for the interpolation scheme in the case of iso-heat-flux condition

$$\Theta_1^k = \tilde{\theta}_5^k + q'' \Delta n / \kappa \tag{14}$$

where $\tilde{\theta}_5^k$ is obtained from the linear interpolation between $\tilde{\theta}_2^k$ and $\tilde{\theta}_3^k$ or $\tilde{\theta}_3^k$ and $\tilde{\theta}_4^k$ (Fig. 5).

Once Θ_1^k is obtained from Eq. (14), the heat source/sink h^k of satisfying the iso-heat-flux condition on the immersed boundary is determined from Eq. (10).

3. Numerical Examples

3.1 Forced convection around a circular cylinder

Forced convection around a circular cylinder is simulated to verify the accuracy of the present immersed boundary method (Gr=0 in Eq. (1)). Both the iso-thermal and iso-heat-flux conditions on the immersed boundary are considered. The size of the computational domain is $-50<x/d<20$ and $-50<y/d<50$, where x and y are the streamwise and transverse directions, respectively, and d is the diameter of a circular cylinder. The Dirichlet boundary conditions, $u=u_\infty$, $v=0$, and $\theta=\theta_\infty$, are used at the inflow and farfield boundaries, and the convective boundary conditions, $\partial u_i/\partial t + c\partial u_i/\partial x = 0$ and $\partial\theta/\partial t + c\partial\theta/\partial x = 0$ are used at the outflow boundary, where u and v are the velocity components in x and y directions, respectively, u_∞ is the free-stream velocity, θ_∞ is the free-stream temperature, and c is the space-averaged streamwise velocity at the exit. At the cylinder surface, $u=v=0$, $\theta=\theta_w$, for the iso-thermal condition and $-\kappa\partial\theta/\partial n = q''$ for the iso-heat-flux condition, where θ_w is the wall temperature, q'' is the wall heat flux and n is the surface-normal direction. The numbers of grid points used are $390(x)\times224(y)$ and thirty grid points in each direction are uniformly distributed within the cylinder. We perform the computations at three different Reynolds numbers (40, 100 and 120) based on the free-stream velocity and diameter. In this paper, air is chosen as a working fluid, so that the Prandtl number is 0.7.

Table 1 Mean Nusselt number for flow over a circular cylinder (iso-thermal condition)

	Re	$\overline{Nu}$
Present	40	3.23
	100	5.13
	120	5.62
Eckert and Soehngen (1952)	40	3.48
	100	5.23
	120	5.69

Table 1 shows the mean Nusselt number (total heat flux) in the case of iso-thermal condition on the cylinder surface, where the total heat flux is obtained from the integration of the heat source/sink over the body and is time-averaged for Re=100 and 120. The present result agrees well with the experimental one by Eckert and Soehngen (1952).

Figure 6 shows the contours of the instantaneous temperature for both the iso-thermal and iso-heat-flux conditions. The temperature field is symmetric about the streamwise axis at Re=40, whereas alternating patterns take place due to the vortex shedding at Re=100 and 120. Differences in the contours are due to the different surface conditions. Fig. 6 indicates that the temperature field is well captured by the present immersed boundary method.

Figure 7 shows the distribution of the Nusselt number ($Nu=h'D/\kappa$, h' is the convection heat transfer coefficient) along the cylinder surface at Re=120 in the case of iso-thermal condition,

together with the experimental result by Eckert and Soehngen (1952). Here, the heat flux at the immersed boundary (i.e. the cylinder surface) is obtained as was done in Fig. 5. Since the grid lines do not coincide with the immersed boundary, one can easily expect some non-smooth patterns in the distribution of Nu as shown in Fig. 7. Nevertheless, the present immersed boundary method captures the heat flux at the cylinder surface very well and shows an excellent agreement with the experimental result.

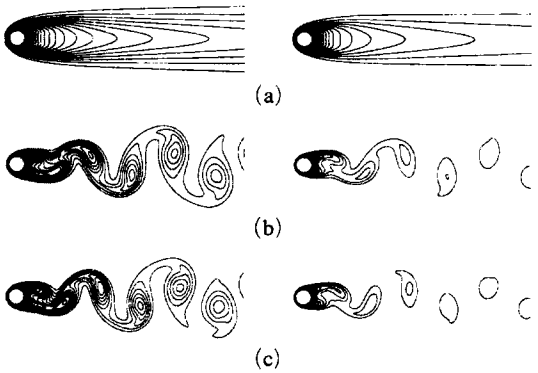

Fig. 6 Contours of the instantaneous temperature: (a) Re=40; (b) Re=100; (c) Re=120. Left figures correspond to the cases of iso-thermal condition and right ones do the cases of iso-heat-flux condition. Contours of the temperature are $(\theta-\theta_w)/(\theta_\infty-\theta_w)=0\sim1$ and κ $(\theta_\infty-\theta)/q''D=0\sim0.3$ for the iso-thermal and iso-heat-flux conditions, respectively

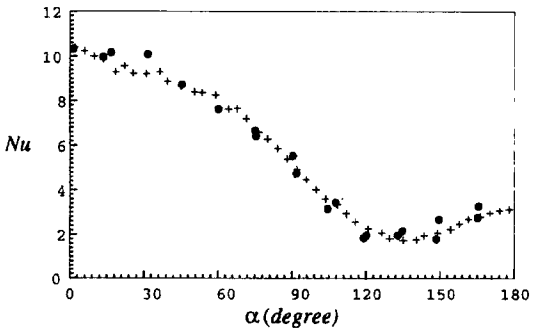

Fig. 7 Distribution of the Nusselt number along the cylinder surface at Re=120 (iso-thermal condition): +, Present; ●, Eckert and Soehngen (1952)

3.2 Mixed convection around a pair of circular cylinders

In this section, we perform the computations for flow and temperature fields around a pair of circular cylinders using a Cartesian mesh. Figure 8 shows the geometry and grid system used in the present computations, where g is the gravitational acceleration, $g^*(=0.7d)$ is the distance between the cylinders, and d is the cylinder diameter. The free-stream direction is opposite to that of the gravity. The size of the computational domain is $-50<x/d<20$, $-50<y/d<50$. The Dirichlet boundary conditions, $u=u_\infty$, $v=0$ and $\theta=\theta_\infty$, are used at the inflow and farfield boundaries, and the convective boundary conditions used in Sec. 3.1 are given at the outflow boundary. At the cylinder surface (immersed boundary), the Dirichlet boundary conditions, $u=v=0$ and $\theta=\theta_w$ are used. The numbers of grid points are $280(x)\times192(y)$ and thirty grid points in each direction are uniformly distributed within the cylinder. Computations are performed for Re=100, Gr=1000, 5000 and 10000, and Pr=0.7 where $\mathrm{Gr}=g\beta(\theta_w-\theta_\infty)d^3/\nu^2$, β is the coefficient of volumetric thermal expansion, and ν is the kinematic viscosity.

Table 2 shows the drag and lift coefficients (C_D and C_L) and the Nusselt number ($\overline{Nu}$) for one cylinder, together with the computational

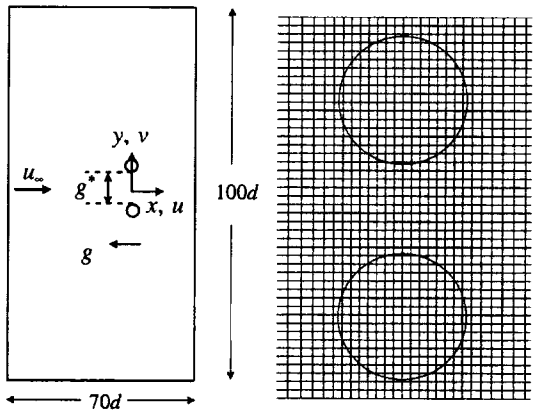

Fig. 8 (a) Coordinate system; (b) Mesh near a pair of cylinders. Here, every other grid lines are shown

Table 2 Drag and lift coefficients and Nusselt number for one cylinder (flow over a pair of circular cylinders)

	Re	Pr	Gr	C_D	C_L	$\overline{Nu}$
Present	100	0.7	1000	1.76	0.39	5.35
			5000	3.02	0.46	5.84
			10000	4.36	0.42	6.36
Song and Chang (1991)	100	0.7	1000	1.80	0.44	5.50
			5000	3.05	0.47	5.75
			10000	4.21	0.44	6.16

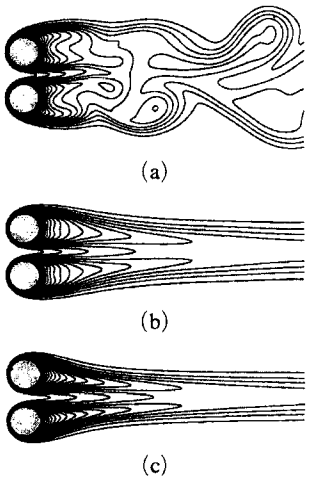

Fig. 9 Temperature contours near a pair of circular cylinders (Re=100): (a) Gr=1000; (b) Gr=5000; (c) Gr=10000

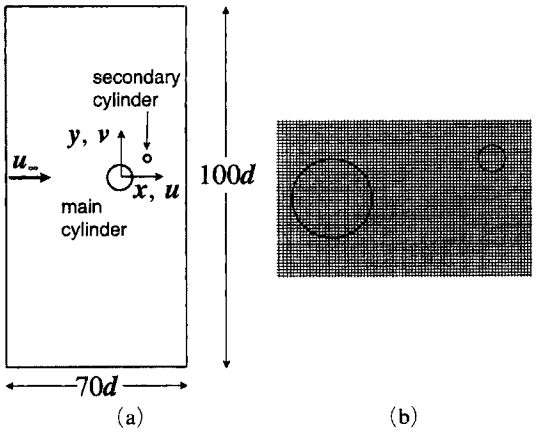

Fig. 10 (a) Coordinate system; (b) Mesh near the two cylinders for the case of $(x_s, y_s)=(2d, 0.5d)$ (every other grid lines are shown here for the mesh of $450(x)\times288(y)$.)

results by Song and Chang (1991). In the case of Gr=1000, flow is unsteady, and thus C_D, C_L, $\overline{Nu}$ are the time-averaged values. As shown, the present results agree well with those by Song and Chang (1991).

Fig. 9 shows the contours of the temperature for Gr=1000, 5000 and 10000 at Re=100. The temperature field changes from unsteady (Gr=1000) to steady (Gr=5000 and 10000) due to the buoyancy force, which agrees well with the numerical results by Song and Chang (1991).

3.3 Forced convection around a main cylinder with a secondary small cylinder

In this section, we simulate forced convection around the main and secondary cylinders at Re=80 and Pr=0.7 (Gr=0). The diameter of the secondary cylinder is $d_s=d/3$ and the secondary cylinder locates at $(x_s, y_s)=(2d, 0.5d)$ or $(2d, 1d)$, where d is the diameter of the main cylinder. This flow configuration was first considered experimentally by Strykowski and Sreenivasan (1990) on the purpose of modifying the vortex shedding and drag.

Figure 10 shows the geometry and grid system. The size of the computational domain is $-50<x/d<20$ and $-50<y/d<50$, and the same boundary conditions as in Sec. 3.2 are used. Two different meshes, $450(x)\times288(y)$ and $900(x)\times576(y)$, are used for the grid-independent solution. For the mesh of $450(x)\times288(y)$, grids of 50×50 are uniformly distributed within the main cylinder, and about 16×16 grid points are uniformly distributed within the secondary cylinder. Twice the grid points are used within the main and secondary cylinders for the mesh of

Table 3 Drag coefficients, lift-coefficient amplitudes and Nusselt numbers for flow over a main cylinder with a secondary small cylinder

		State	C_D	C'_L	C_{D_s}	C'_{L_s}	$\overline{Nu}$	$\overline{Nu_s}$
Without secondary cylinder	Present ($450(x)\times288(y)$)	unsteady	1.37	0.241			4.56	
	Eckert and Soehngen (1952)	unsteady					4.64	
	Strykowski and Sreenivasan (1990)	unsteady						
	Park et al. (1998)	unsteady	1.35	0.245				
$(x_s, y_s)=(2d, 0.5d)$	Present ($450(x)\times288(y)$)	unsteady	1.24	0.0483	0.129	0.0644	4.35	1.19
	Present ($900(x)\times576(y)$)	unsteady	1.24	0.0482	0.130	0.0645	4.36	1.19
	Strykowski and Sreenivasan (1990)	unsteady						
$(x_s, y_s)=(2d, 1d)$	Present ($450(x)\times288(y)$)	steady	1.17	0	0.461	0	4.36	2.34
	Present ($900(x)\times576(y)$)	steady	1.17	0	0.461	0	4.36	2.34
	Strykowski and Sreenivasan (1990)	steady						

$900(x)\times576(y)$. In this study, we consider two different locations for the secondary cylinder: $(x_s, y_s)=(2d, 0.5d)$ and $(2d, 1d)$. Here, the first and the latter produce, respectively, maintenance and suppression of vortex shedding according to the experiments by Strykowski and Sreenivasan (1990).

Table 3 shows the drag coefficients, lift-coefficient amplitudes and the Nusselt numbers, together with those from the previous studies (Eckert and Soehngen, 1952; Strykowski and Sreenivasan, 1990; Park et al., 1998). Here C_D, C'_L and $\overline{Nu}$ are the drag coefficient, lift-coefficient amplitude and the Nusselt number of the main cylinder, respectively, and C_{D_s}, C'_{L_s} and $\overline{Nu_s}$ are those of the secondary cylinder. These values are normalized by u_∞ and d. As shown in Table 3, the present results are in good agreements with the previous experimental (Eckert and Soehngen, 1952; Strykowski and Sreenivasan, 1990) and numerical (Park et al., 1998) results. As shown in Table 3, the drag coefficients, lift-coefficient amplitudes and the Nusselt numbers are nearly the same for both grids, indicating that the solutions are grid-independent.

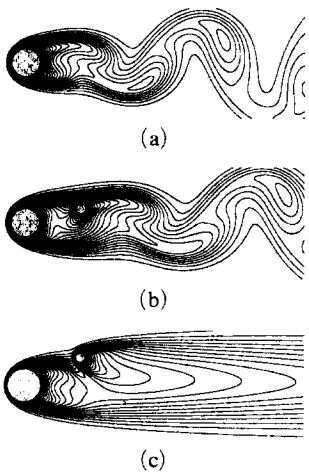

Fig. 11 Temperature contours behind a main cylinder with a secondary small cylinder (Re=80): (a) Without secondary cylinder; (b) $(x_s, y_s)=(2d, 0.5d)$; (c) $(x_s, y_s)=(2d, 1d)$

With the secondary cylinder, the drag and heat transfer on the main cylinder are reduced. However, the total drag $(=C_D+C_{D_s})$ is nearly the same for $(x_s, y_s)=(2d, 0.5d)$ and is increased for $(2d, 1d)$. The total heat fluxes $(=\overline{Nu}+\overline{Nu_s})$ are increased for both cases. On the other hand, the lift fluctuations are reduced and completely eliminated for $(x_s, y_s)=(2d, 0.5d)$ and $(2d, 1d)$, respectively, due to the delay or complete suppression of vortex shedding with the secondary cylinder (see Fig. 11). These behaviors are similar to those reported in Strykowski and Sreenivasan (1990). Fig. 11 clearly shows that the present immersed boundary method accurately captures the thermal field.

4. Summary

In the present study, an immersed boundary method was presented for the simulation of heat transfer inside/over a complex geometry by introducing the heat source/sink as well as both the momentum forcing and mass source/sink. The present method was based on a finite volume approach on a staggered mesh together with a fractional step method. The heat source/sink was applied on the immersed boundary or inside the body to satisfy the thermal boundary conditions (iso-thermal and iso-heat-flux conditions) on the immersed boundary. In the present method, accurate interpolation schemes were developed to satisfy the iso-thermal and iso-heat-flux conditions on the immersed boundary.

Three different heat transfer problems (forced convection around a circular cylinder, mixed convection around a pair of circular cylinders, and forced convection around a main cylinder with a secondary small cylinder) were solved using the present immersed boundary method. The simulation results agreed well with the previous numerical and experimental ones, verifying the accuracy of the present immersed boundary method.

Acknowledgment

This work is supported by the Creative Research Initiatives of the Korean Ministry of Science and Technology and BK21 program of the Korean Ministry of Education and Human Resources Development.

References

Eckert, E. R. G. and Soehngen, E., 1952, "Distribution of Heat-Transfer Coefficients Around Circular Cylinders in Crossflow at Reynolds Numbers from 20 to 500," *Trans. ASME*, Vol. 75, pp. 343~347.

Fadlun, E. A., Verzicco, R., Orlandi, P. and Mohd-Yusof, J., 2000, "Combined Immersed-Boundary Finite-Difference Methods for Three-Dimensional Complex Flow Simulations," *J. Comput. Phys.*, Vol. 161, pp. 35~60.

Goldstein, D., Handler, R. and Sirovich, L., 1993, "Modelling a No-Slip Flow Boundary with an External Force Field," *J. Comput. Phys.*, Vol. 105, pp. 354~366.

Kim, J., Kim, D. and Choi, H., 2001, "An Immersed-Boundary Finite-Volume Method for Simulations of Flow in Complex Geometries," *J. Comput. Phys.*, Vol. 171, pp. 132~150.

Lee, C., 2003, "Stability Characteristics of the Virtual Boundary Method in Three-Dimensional Applications," *J. Comput. Phys.*, Vol. 184, pp. 559~591.

Mohd-Yusof, J., 1997, "Combined Immersed-Boundary/B-Spline Methods for Simulations of Flow in Complex Geometries," *Annual Research Briefs*, Center for Turbulence Research, NASA Ames and Stanford University.

Park, J., Kwon, K. and Choi, H., 1998, "Numerical Solutions of Flow Past a Circular Cylinder at Reynolds Numbers up to 160," *KSME Int. J.*, Vol. 12, pp. 1200~1205.

Peskin, C. S., 1982, "The Fluid Dynamics of Heart Valves: Experimental, Theoretical and Computational Methods," *Annu. Rev. Fluid Mech.*, Vol. 14, pp. 235~259.

Saiki, E. M., and Biringen, S., 1996, "Numerical Simulation of a Cylinder in Uniform Flow: Application of a Virtual Boundary Method," *J. Comput. Phys.*, Vol. 123, pp. 450~465.

Song, C.-J. and Chang, K.-S., 1991, "Heat Transfer and Interactive Buoyant Vortex Shed-

ding by a Pair of Circular Cylinders in Transverse Arrangement," *Int. J. Heat Mass Transfer*, Vol. 34, No. 6, pp. 1347~1354.

Strykowski, P. J. and Sreenivasan, K. R., 1990, "On the Formation and Suppression of Vortex Shedding at Low Reynolds Numbers," *J. Fluid Mech.*, Vol. 218, pp. 71~107.